ACS APPLIED ENERGY MATERIALS

www.acsaem.org Article

Enhancing Li-Ion Conductivity in $LiBH_4$-Based Solid Electrolytes by Adding Various Nanosized Oxides

Valerio Gulino,[#] Laura Barberis,[#] Peter Ngene, Marcello Baricco,[*] and Petra E. de Jongh[*]

Cite This: *ACS Appl. Energy Mater.* 2020, 3, 4941−4948 Read Online

ACCESS | Metrics & More | Article Recommendations | Supporting Information

ABSTRACT: Solid-state ion conductors are gaining increasing importance, among other ion conductors, to enable a transition to next-generation all-solid-state Li batteries. However, few lightweight and low-cost materials show sufficiently high Li-ion conduction at room temperature to be used as solid electrolytes. Here, we report the effect of adding nanosized oxides, SiO_2, CaO, MgO, γ-Al_2O_3, TiO_2, and ZrO_2, to $LiBH_4$ by ball-milling. In all cases, the room temperature Li-ion conductivity was greatly enhanced. For SiO_2, which has been reported before as a conductivity enhancing material, the highest conductivity (4.1×10^{-5} S/cm at 40 °C) and the lowest activation energy (0.49 eV) were found at 20 v/v% SiO_2. For the first time, ZrO_2 and MgO were also added to $LiBH_4$, leading to more than a 4 orders of magnitude increase in conductivity at 40 °C, reaching 0.26 and 0.18 mS/cm, respectively. Based on insights into the effect of structural properties on conductivity, we present a set of general guidelines to maximize the Li-ion conductivity in these nanocomposite solid electrolytes, independently of the type of oxide added. We expect that these results and insights will be helpful for the further development of new room temperature solid-state ion conductors.

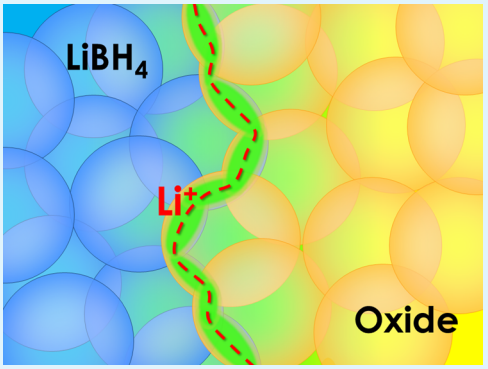

KEYWORDS: *ionic conductivity, nanocomposites, lithium-ion batteries, solid electrolytes, complex metal hydrides*

INTRODUCTION

The main goals in the current research in the battery field is to increase safety and energy density. Present Li-ion battery electrolytes typically consist of lithium salts dissolved in organic solvents.[1] Solid-state electrolytes could improve the safety, thermal stability, and capacity of Li-ion batteries,[2,3] resolving the risks associated with flammable organic solvents and increasing the lifetime of the devices.[4] Different classes of materials have been studied as solid-state ion conductors, including complex hydrides.[5−8] Lithium borohydride ($LiBH_4$) is one of the candidate complex hydrides for this application, in view of its low density (0.666 g/cm^3) and electrochemical stability (close to 2 V vs. Li^+/Li).[9,10] The orthorhombic low-temperature (LT) phase, with space group (s.g.) *Pnma*, shows a rather low ionic conductivity (around 10^{-8} S/cm) at room temperature (RT).[11,12] Because of a structural transformation at 110 °C from the LT phase to a high-temperature (HT) hexagonal phase, (s.g. $P6_3mc$),[12] the Li-ion conductivity of $LiBH_4$ increases by almost 3 orders of magnitude. A superionic conductivity for the HT structure, e.g., ~10^{-3} S/cm at 120 °C, was first reported by Matsuo et al.[11] The challenge for the development of solid-state electrolytes based on $LiBH_4$ is to extend the high ionic conductivity of the HT hexagonal phase to lower temperatures, i.e., down to RT, or to enhance the Li-ion conductivity of the LT orthorhombic phase.

The HT phase of $LiBH_4$ has been stabilized at RT by mixing it with lithium halides (e.g., LiI, LiBr, LiCl) to form solid solutions.[10,13−17] Also, the combination of $LiBH_4$ with other complex hydrides (e.g., $LiNH_2$ and Li_2NH) stabilizes new compounds that demonstrate an improved Li-ion conductivity at RT.[18−20] A different approach to increase the ionic conductivity of the LT phase of $LiBH_4$ is by mixing it with oxides to form a composite, e.g., by nanoconfinement in suitable scaffolds.[21−26] Blanchard et al.[27] reported the effect of $LiBH_4$ confinement on Li-ion conductivity and mobility using an ordered mesoporous silica scaffold (MCM-41). In order to explain the increase of the ionic conductivity of composites, a core−shell model was proposed, considering two different fractions of $LiBH_4$ present in the pores. The first fraction is positioned in the center of the pores, and upon heating, similarly to bulk $LiBH_4$, it undergoes a transition to the solid phase but at lower temperatures.[27] The second fraction, which does not undergo a solid−solid phase transition, is located at the interface layer between $LiBH_4$ and SiO_2, and it is

Received: March 7, 2020
Accepted: April 30, 2020
Published: April 30, 2020

https://dx.doi.org/10.1021/acsaem.9b02268
ACS Appl. Energy Mater. 2020, 3, 4941−4948

responsible for the high ionic conductivity. Suwarno et al.[26] quantified the thickness of the high-mobility layer at the interface, which corresponds to 1.94 ± 0.13 nm for a silica nanoscaffold.

Afterward, Choi et al.[21,22] prepared $LiBH_4$−oxide nanocomposites by ball-milling, followed by a heat treatment above the $LiBH_4$ melting point. Electrochemical impedance results obtained for nanocomposites with both SiO_2 and Al_2O_3 demonstrated that the Li-ion conductivity of $LiBH_4$ can be enhanced. The exact mechanism leading to the increase in Li-ion conduction is not fully understood yet. However, it has been suggested that the nanostructure created at the interface by the interaction of $LiBH_4$ with the oxide generates a fraction of material characterized by preferential pathways for ion conduction.[22,26,28] NEXAFS spectroscopy was employed to explore possible interface changes after ball-milling, by analyzing the chemical bonding of the constituent elements.[22] A new chemical bond between B and O was identified from NEXAFS spectra, meaning that some oxidation takes place at the interface. The number of B−O bonds could not be linked to the increase of conductivity, but it is clear that Al_2O_3 and SiO_2 are not completely inert during ball-milling with $LiBH_4$.[22,29]

In the past decades, several composite ionic conductors have been synthesized by mixing Li-based compounds with an insulator phase, e.g., Li_2O-ion conductivity has been enhanced by mixing with Al_2O_3 and B_2O_3.[30−32] Frequency- and temperature-dependent ^{7}Li solid-state NMR spectroscopy measurements performed on different two-phase composites demonstrated heterogeneous dynamics, reflecting the presence of slow and fast diffusing Li ions, in accordance with the space-charge layer effect,[33,34] which corresponds to carrier redistribution at space-charge regions near a two-phase interface. The presence of an insulator could create a defective and highly conducting layer along the interface between the conducting and the insulating phases.[35] However, high mobilities and two different phases were also detected when mixing with conductive carbon powder.[36]

As described above, creating interfaces with an oxide is a successful strategy to increase the Li-ion conductivity of $LiBH_4$ at RT, but it is not yet fully understood. So, this work is aimed at synthesizing novel solid-state fast ionic conductors based on $LiBH_4$−oxide systems. The synthesis of nanocomposites was obtained by ball-milling, without any heat treatment afterward. The effect on Li-ion conductivity of mixing $LiBH_4$ with different oxides has been investigated. For all samples prepared, the Li-ion conductivity was at least 3 orders of magnitude higher than that observed for the as-received $LiBH_4$, and the fast Li-ion conductivity was stable up to about 130 °C. Varying the ratio between SiO_2 and $LiBH_4$ and changing the oxide yielded new insights on how the enhanced conductivity correlates with structural properties of nanocomposites.

EXPERIMENTAL SECTION

$LiBH_4$ (purity > 95% from Alfa Aesar) was mixed in different v/v% ratios with oxides (see Table 1). SiO_2 (Aerosil 300, Evonik), CaO (Steam Chemicals), MgO (Steam Chemicals), Al_2O_3 (γ-phase, Alfa Aesar), TiO_2 (P90, Evonik), and ZrO_2 (RC 100, Gimex) were pelletized and dried at 300 °C in a furnace, under dynamic vacuum, for 6 h. All sample manipulations were performed in an argon-filled glovebox (MBraun Lab Star Glove Box supplied with pure 5.5 grade argon, <1 ppm of O_2, <1 ppm of H_2O).

Table 1. Composition of Investigated Mixtures[a]

oxide	oxide	oxide	ρ[37]	BET surface area	V_p	fraction of pore filled[b]	thickness of $LiBH_4$[c]
	wt.%	v/v%	g/cm^3	m^2/g	cm^3/g	%	nm
SiO_2	30	11	2.20	294	2.30	152	11.9
SiO_2	45	20	2.20	294	2.30	80	6.2
SiO_2	55	27	2.20	294	2.30	53	4.2
SiO_2	63	34	2.20	294	2.30	38	3.0
SiO_2	70	41	2.20	294	2.30	28	2.2
SiO_2	78	52	2.20	294	2.30	18	1.4
ZrO_2	75	25	5.89	94	0.26	193	5.3
TiO_2	68	25	4.10	94	0.48	147	7.5
Al_2O_3	67	25	3.96	67	0.30	247	11.0
MgO	65	25	3.58	215	0.25	323	3.8
CaO	62	25	3.30	20	0.13	708	46.0

[a]The measured values of the surface area are in agreement with the information provided by the manufacturer; see Experimental Section for the measurement conditions. [b]Calculation performed dividing the $LiBH_4$ occupied volume per gram of SiO_2 by the pore volume (V_p). [c]Calculation performed considering the BET surface area of the oxides and assuming it a flat geometry.

A Fritsch Pulverisette 6 planetary mill was used to ball mill the starting materials in 80 mL tungsten carbide vials, with tungsten carbide balls (10 mm outside diameter). The balls-to-sample mass ratio used was 30:1. The mechanochemical treatment was performed under argon atmosphere for all samples. Before mixing, as-received $LiBH_4$ was ball-milled for 2 h at 500 rpm and the effect of the mechanochemical treatment on the Li-ion conductivity was evaluated. The ball-milled $LiBH_4$ was used as the starting material for the $LiBH_4$−oxide mixtures. All samples prepared were milled for three periods of 10 min at 300 rpm. Breaks of 2 min have been used between each period in order to overcome heating effects. Samples with different oxides were prepared with the same volume fraction (~25 v/v% of oxide) (see Table 1).

The surface areas (S_{BET}) and total pore volumes (V_p) of different oxides (see Table 1) were obtained by N_2 adsorption at 77 K in a TriStar Plus II gas-volumetric apparatus (Micromeritics, Norcross, GA, USA). The specific surface areas of different oxides were derived by fitting with a Brunauer−Emmett−Teller isotherm,[38] whereas the total pore volume was obtained from the absorbed volume of the nitrogen at $p/p_0 = 0.95$.

The Li-ion conductivity was measured by electrochemical impedance spectroscopy (EIS) using a PARSTAT 2273 potentiostat (frequency range 1 Hz/1 MHz, applied voltage 10 mV), with the measuring cell placed inside an Ar-filled glovebox. Samples were compacted into pellets (diameter 13 mm, thickness 1−2 mm) using an axial hydraulic press with about 200 MPa pressure. Lithium foils (Sigma-Aldrich, purity 99.9%, 0.38 mm thick) were used as nonblocking electrodes. EIS was performed every 10 °C in the temperature range of RT < T < 130 °C during the heating ramp, probing every 20 °C during cooling. Different EIS temperature-dependent cycles were performed to verify the reproducibility and the stability of measurements. At each set point, a dwell time of about 50 min was used for the pellet temperature to equilibrate. The impedance spectra showed a single arc in the Nyquist plot; therefore, the bulk and interface properties were modeled with a constant phase element in parallel with a resistor. The Li-ion conductivity was calculated from the ratio of the thickness of the sample and the resistance obtained from the fit of EIS multiplied by the area of the pellet. Impedance data were analyzed via the EqC software,[39] following the data validation described in ref 40. All performed fits resulted in $\chi^2 < 10^{-3}$.

https://dx.doi.org/10.1021/acsaem.9b02268
ACS Appl. Energy Mater. 2020, 3, 4941−4948

EFFECT OF BALL-MILLING ON LI-ION MOBILITY OF $LiBH_4$

The effect of the mechanical treatment on the Li-ion mobility was first evaluated by ball-milling the as-received $LiBH_4$ for 2 h at 500 rpm. Figure 1 shows the Arrhenius plot of the ionic conductivity of as-received and ball-milled $LiBH_4$, measured by EIS. Two cycles are reported for the ball-milled sample, in order to clarify the effect of the temperature cycling on the Li-ion conductivity. For the as-received $LiBH_4$, only the second cycle is reported. The first and the second temperature-dependent EIS cycles of as-received $LiBH_4$ are shown in Figure S1. The Nyquist plot and the equivalent circuit used to fit the data for the as-received and ball-milled $LiBH_4$ are reported in Figure S2.

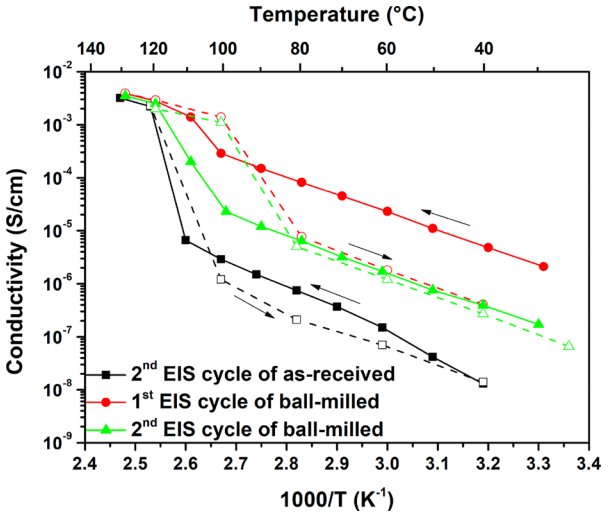

Figure 1. Li-ion conductivity of the second temperature-dependent EIS cycle of as-received $LiBH_4$ (black squares) as well as the first and second temperature-dependent EIS cycles of ball-milled $LiBH_4$ (red circles and green triangles, respectively). Closed symbols and solid lines correspond to the heating ramp, while open symbols and dashed lines represent the cooling.

Below 120 °C, ball-milled $LiBH_4$ shows much higher ionic conductivities, i.e., 4.8×10^{-6} S/cm at 40 °C for the first cycle and 3.9×10^{-7} S/cm for the second cycle, than the as-received sample, 1.3×10^{-8} S/cm. Values obtained at 30 °C are presented in Table S1. The Li-ion conductivity of the ball-milled sample during the first cycle is about 3 orders of magnitude higher than that of the as-received $LiBH_4$. However, the ionic conductivity is much lower during the subsequent cooling ramp. The Li-ion conductivity measured during the second cycle is similar to that measured during the cooling ramp of the first cycle. The high conductivity detected directly after ball-milling is probably due to structural modifications, most notably because of an increase of defects due to the mechanochemical treatment. The XRD pattern of ball-milled $LiBH_4$ (Figure S3) shows marginally broader diffraction peaks than those of as-received $LiBH_4$. This can be ascribed to a reduction of crystallite size and/or introduction of strain in the crystal lattice. Differential scanning calorimetry (DSC) analysis of as-received and ball-milled LiBH4 (Figure S4) shows the expected LT-to-HT reversible phase transition around 110 °C, explaining the conductivity increase observed in Figure 1. In addition, the DSC traces show a hysteresis of about 15 °C, in agreement with that observed in the conductivity measurements where a measurement point was taken every 20 °C.

The temperature dependence of ionic conductivity (σ) can be described by

$$\sigma(T) = \frac{\sigma_0}{T} e^{-E_A/k_B T} \quad (1)$$

where E_A is the activation energy, k_B is the Boltzmann constant, and σ_0 is a pre-exponential factor. The activation energy was obtained by a linear fit of the data shown in Figure 1 with eq 1, considering the heating ramps below the transition temperature. Values equal to 0.70, 0.75, and 0.91 eV were determined for the first and second cycles of ball-milled $LiBH_4$ and the second cycle of as-received $LiBH_4$, respectively. The activation energy for the ball-milled $LiBH_4$ is smaller than that obtained for the as-received $LiBH_4$, but it increases upon heat thermal cycling.

An increase of the Li-ion conductivity of $LiBH_4$ due the mechanochemical treatment was already reported in the

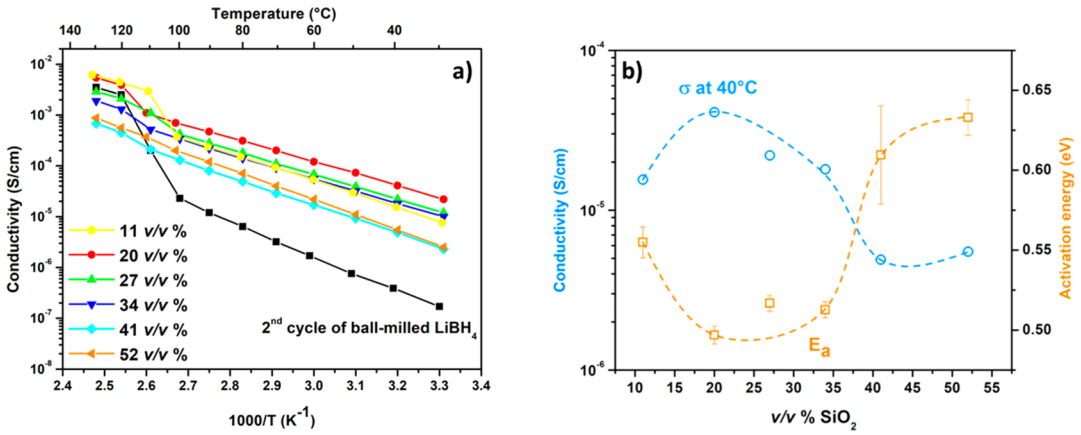

Figure 2. (a) Li-ion conductivity of samples containing different v/v% ratios of SiO_2. All data were obtained from the second heating temperature-dependent EIS cycle. Li-ion conductivity of the ball-milled $LiBH_4$ during the second heating temperature-dependent EIS cycle is shown for comparison. (b) Li-ion conductivity at 40 °C and activation energy as a function of the v/v% of SiO_2. The activation energy was calculated from data collected during the second heating ramp. Error bars were obtained from the linear fit of the Arrhenius plot (95% of confidence). Dashed lines are a guide for the eye.

https://dx.doi.org/10.1021/acsaem.9b02268
ACS Appl. Energy Mater. 2020, 3, 4941−4948

literature (see Figure S5).[17,41] Ball-milling increases the defect concentration, leading to an increase of the number of Li interstitials and Li vacancies, which are relevant for Li-ion mobility.[42] Recently, Breuer et al.,[43] using ^{7}Li longitudinal nuclear magnetic relaxation, could detect two different mobility mechanisms of Li ion in nanocrystalline orthorhombic $LiBH_4$. The surface pathways through defective regions offer activation barriers much lower than those in the crystalline bulk regions.[44] However, the ionic conductivity decreases by 1 order of magnitude after heating up to the phase transition temperature, presumably because of the annihilation of some defects caused by the mechanochemical treatment, which facilitated the Li-ion mobility. This means that, although ball-milling can induce an increase of conductivity, it depends on nonstable defects, that disappear mostly upon heat treatment. It would therefore be very interesting to find a way to stabilize the enhanced Li-ion conductivity. For this reason, the effect of the composition on Li-ion conductivity in the $LiBH_4$−SiO_2 mixed system was analyzed.

$LiBH_4$−SiO_2 COMPOSITES: INFLUENCE OF THE COMPOSITION

The effect of the composition on Li-ion conductivity in $LiBH_4$−SiO_2 has been evaluated for a composition range (from 11 to 52 v/v% of silica) corresponding to a pore filling fraction from 18 to 152% (see Table 1). After the synthesis, an XRD analysis was performed at RT for each sample, confirming that no new compounds had been formed (Figure S6). The Arrhenius plots for the conductivity of ball-milled samples with different v/v% ratios of SiO_2 are shown in Figure 2a. Values obtained at 30 °C are presented in the Table S1. As an example, the Nyquist plot and the equivalent circuit used to fit the data for the as-received and ball-milled $LiBH_4$ are reported in Figure S7.

In the low-temperature range, below 110 °C, the conductivity values for all composite samples are higher than those obtained for the orthorhombic as-received $LiBH_4$. Among all samples, those with 20 v/v% of SiO_2 show the highest ionic conductivity in the whole temperature range before the phase transition. Observed values of Li-ion conductivity are close to those reported by Choi et al.[21] (1.5×10^{-5} S/cm at 40 °C for 55 v/v% of fumed silica) and by Blanchard et al.[27] (1.0×10^{-5} S/cm at 40 °C for 28 v/v% of MCM-41).

In Figure 2a, the sudden change of Li-ion conductivity due to the LT-to-HT phase transition is not always observed. Data for 41 and 52 v/v% SiO_2 mixtures do not show the jump due to the formation of the HT phase, suggesting that the conductive contribution by the bulk $LiBH_4$ in the samples is negligible. On the other hand, around the phase transition temperature, 27 and 34 v/v% SiO_2 samples exhibit a slight change in conductivity, and samples containing 11 and 20 v/v % of SiO_2 show an evident jump of the Li-ion conductivity at about 110 °C. In 11 and 20 v/v% SiO_2 samples, above the phase transition, the Li-ion conductivity is higher with respect to the conductivity measured for the hexagonal phase of the as-received $LiBH_4$, meaning that a synergic effect is still observed.

Suwarno et al.[26] demonstrated, by pore-size-dependent transition enthalpy measurements, that a fraction of the $LiBH_4$, which is in direct contact with the SiO_2, does not undergo a structural phase transition. The thickness of this interface layer was estimated as 1.94 ± 0.13 nm.[26] The enhancement of Li-ion conductivity due to the phase transition in samples containing silica could be explained considering the estimated values for the thickness of the $LiBH_4$ layer on SiO_2 (see Table 1). The calculation was performed taking into account the surface area of the SiO_2 and assuming that its surface is fully and uniformly covered by $LiBH_4$. Indeed, for samples with 41 and 52 v/v% SiO_2, which do not show the jump of the Li-ion conductivity associated with the phase transition, the calculated thickness of $LiBH_4$ (2.2 and 1.4 nm, respectively) is close to the value estimated by Suwarno et al.[26] Considering other samples, the calculated thickness is higher than that estimated for the high conductive interface layer, confirming the contribution to Li-ion conductivity from crystalline $LiBH_4$. Data reported by Choi et al.[21] are in agreement with this behavior, i.e., the samples with a calculated $LiBH_4$ thickness lower that about 2 nm do not show an increased Li-ion conductivity after the phase transition.

Figure 2b shows the Li-ion conductivity at 40 °C as a function of the amount of silica. A maximum is reached for the sample with 20 v/v% of SiO_2 (4.1×10^{-5} S/cm), with samples containing 27 and 34 v/v% of SiO_2 showing conductivity values close to this maximum. A clear decrease of Li-ion conductivity is observed for higher loadings (41 and 52 v/v% of SiO_2). In Figure 2b, the dependence of the activation energy as a function of the amount of silica is also included. The lowest value of activation energy is observed for the sample containing 20 v/v% of SiO_2 (i.e., 0.49 eV), which, compared to the value of 0.91 eV obtained for pure $LiBH_4$, may be linked to the increased conductivity due to the formation of the composite. An increase of the amount of silica in the mixture led to higher values for the activation energy as well as for the sample containing 11 v/v% of SiO_2. Obtained activation energy values are close to those reported in the literature for similar composite conductors.[21,27] Figure S8 shows the correlation between Li-ion conductivity and activation energy, where lower activation energies correspond to a higher Li-ion conductivity.

We also analyzed in detail the relation between conductivity and the fraction of pores filled. Figure 3 reports the conductivity at 40 °C for $LiBH_4$−SiO_2 composites as a function of pore filling. Pore filling is here defined as the ratio between the volume of the pores in the oxide powder before

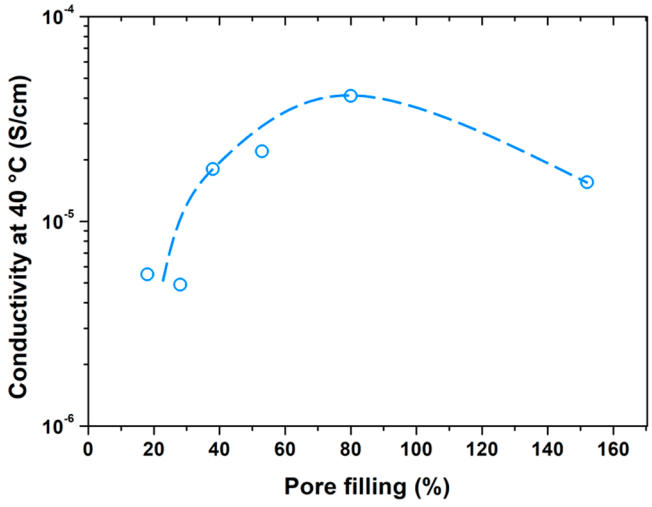

Figure 3. Li-ion conductivity at 40 °C as a function of pore filling (%).

https://dx.doi.org/10.1021/acsaem.9b02268
ACS Appl. Energy Mater. 2020, 3, 4941−4948

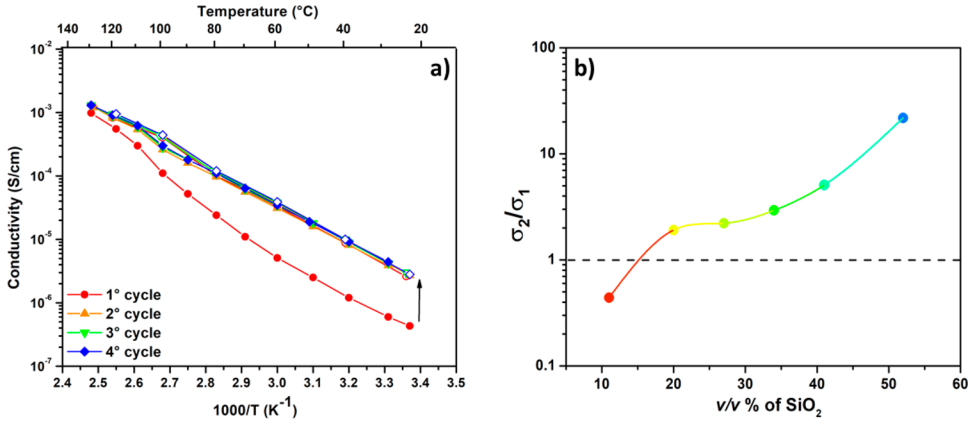

Figure 4. (a) Arrhenius plot of the BM samples with 41 v/v% of SiO_2 cycled from 30 to 130 °C four times. Closed symbols represent the heating ramp, and open symbols represent the cooling. (b) Ratio between the conductivity measured at 40 °C for the second and first heating ramps as a function of the v/v% of SiO_2.

the addition of the $LiBH_4$ and the volume of the $LiBH_4$ added. As the oxides consist of nanocrystallites, it is not expected that ball-milling will greatly modify the effective mesopore volume, which is formed by the interparticle space between the crystallites. SiO_2 itself is an insulator, so without $LiBH_4$ (0% pore filling), the conductivity is negligible. Upon increasing the fraction of interparticle volume filled, the conductivity rapidly increased, most likely because gradually a connected pathway for Li ions (conducting regions) is formed. The highest Li-ion conductivity was found for the the sample closest to a complete pore filling. The conductivity increases with the increasing of pore volume filling and decreases after exceeding the complete pore filling. For the first time, we report a clearly structural parameter that maximizes the Li-ion conductivity.

The occurrence of an optimal volume fraction of insulating material and pore filling that maximizes the conductivity, as shown in Figures 2 and 3, can be explained considering two forms of $LiBH_4$ (the "core-shell model"[27]), in which highly conductive $LiBH_4$ (the "shell") is within a short distance from the interface with the oxide, while bulk $LiBH_4$, which is further away from the interface (the "core"), has a much lower conductivity at room temperature. In the sample with 11 v/v% SiO_2, an excess of crystalline $LiBH_4$ is present (pore filling "150%"); therefore, the conduction pathway of the highly conductive phase is interrupted by the lower-conductivity crystalline $LiBH_4$ regions. On the contrary, in samples containing SiO_2 > 20 v/v%, where the pore filling is below 100%, it is the insulating oxide or void regions that interrupt the Li-ion pathway. A tailoring of the pore filling allows the volume ratio between the highly conductive interface layer and bulk $LiBH_4$ to be optimized. Consequently, a deviation from a complete filling of pores in the composite (thus for both too-low- and high-volume fractions of insulating materials) cannot provide a well-connected interface layer network. This is the first time that the optimum ratio of ion conductor and oxidic additive has been clearly related to an easily measurable structural parameter, the pore volume of the oxide additive powder. We look forward to its validity being scrutinized by future results (for instance, Choi et al.[21] reported a maximum value of Li-ion conductivity for a $LiBH_4$–SiO_2 composite with 55 v/v% of fumed silica but did not mention the pore volume of the oxide powder).

EFFECT OF HEAT TREATMENT

The ionic conductivity for each sample was measured during four subsequent heating/cooling cycles. For the whole composition range, the conductivity increased after the first heating ramp, but from the second cycle, the Li-ion conductivity remained basically constant. As an example, the Arrhenius plot obtained for the sample with 41 v/v% of silica is shown in Figure 4a, where an increase by 1 order of magnitude after the first heating step was observed. The ratio between conductivities measured at 40 °C in the first and the second heating ramps increased as a function of the added amount of SiO_2, as reported in Figure 4b. The increase of the ionic conductivity after the first heating ramp in nanocomposites with a high amount of silica is the opposite of that observed for the pure ball-milled $LiBH_4$ (compare with Figure 1). In fact, this behavior was observed for all mixtures, except for the sample containing 11 v/v% of SiO_2, where the conductivity decreased after the first cycle (Figure 4b).

The observed behavior can be explained considering the first heating cycle as a heat treatment. Following this heat treatment, defects deriving from the mechanochemical treatment are annihilated in the bulk $LiBH_4$. The behavior observed for the sample with only 11 v/v% of silica resembles that observed for ball-milled $LiBH_4$, indicating that for this sample the observed conductivity is dominated by the macrocrystalline $LiBH_4$. On the contrary, the formation of the highly conductive interface region at the $LiBH_4$/oxide interface seems to be promoted and stabilized by heat treatment, giving the highly conductive nanocomposites an excellent resistance against temperature fluctuations.

EFFECT OF DIFFERENT OXIDES ON THE LI-ION MOBILITY IN $LiBH_4$

In the literature, a high ionic conductivity has been reported for $LiBH_4$ nanocomposites obtained not only with silica but also with alumina.[22] Here, we present a systematic study of the influence of different types of oxides, both insulators, such as CaO, MgO, and ZrO_2, as well as semiconductors, such as TiO_2. Before milling, the same pretreatment conditions were applied for all oxides, as it is known from $LiBH_4$/SiO_2 nanocomposites that pretreatment of the oxide can influence the conductivity of the nanocomposite.[45] In all cases, 25 v/v% of oxide in the mixture was added (see Table 1). The XRD patterns show no evidence for any additional crystalline

https://dx.doi.org/10.1021/acsaem.9b02268
ACS Appl. Energy Mater. 2020, 3, 4941−4948

compounds other than the starting components (Figures S9–S13). The resulting Li-ion conductivities, derived from EIS during the second heating ramp for composites containing different oxides, are shown as an Arrhenius plot in Figure 5.

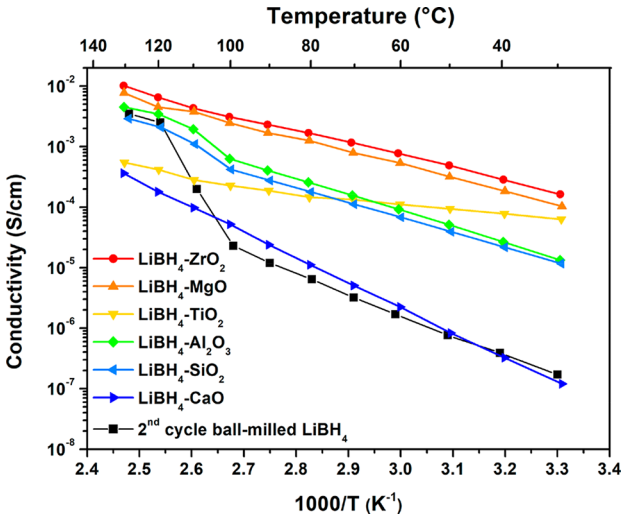

Figure 5. Li-ion conductivity of ball-milled mixtures of $LiBH_4$ with 25 v/v% of different oxides. All data shown were obtained during the second heating temperature-dependent EIS cycle. Li-ion conductivity of the ball-milled $LiBH_4$ and the sample containing 27 v/v% of SiO_2, during the second heating temperature-dependent EIS cycle, is shown for comparison.

Values obtained at 30 °C are presented in the Table S1. The Nyquist plot and the equivalent circuit used to fit the data for the samples containing different oxides are reported in Figures S14 and S15.

All samples show a Li-ion conductivity higher than that of as-received $LiBH_4$. The $LiBH_4$–CaO mixture shows the lowest ionic conductivity in the whole temperature range, with a value equal to 1.6×10^{-6} S/cm at 40 °C. However, this might also be caused by the fact that, due to the low pore volume of CaO, in this case, about 7 times more $LiBH_4$ is added than corresponding to the pore volume. Very interestingly, the ionic conductivity reaches 0.26 and 0.18 mS/cm at 40 °C for samples containing ZrO_2 and MgO, respectively. These values are more than 4 orders of magnitude higher than that obtained for the as-received $LiBH_4$ and also clearly higher than those observed for nanocomposites with SiO_2 and Al_2O_3. The lowest activation energies, 0.44 and 0.46 eV, were observed for samples containing ZrO_2 and MgO, respectively, while samples containing CaO, SiO_2, and Al_2O_3 show activation energies equal to 0.86, 0.52, and 0.55 eV, respectively.

The mixture of $LiBH_4$ with TiO_2 shows a strikingly low activation energy (0.24 eV). The color of the nanocomposite was blue. TiO_2 is the only oxide in the series that is not an insulator but a semiconductor, and it is known that the blue color is caused by the presence of Ti^{3+} and oxygen defects.[46] Since $LiBH_4$ is a strong reducing agent, it is likely that some TiO_2 has been reduced by the $LiBH_4$ forming TiO_{2-x}. In the partially reduced form, titanium dioxide has an appreciable electronic n-type conductivity.[47] The conductivity as measured by electrochemical impedance is the sum of (cat- and an-)ionic conductivity and electronic conductivity. To separate the two components, the electronic conductivity of the samples containing ZrO_2, MgO, and TiO_2 has been evaluated by DC voltage polarization,[48,49] and the results are reported in Figure S16. For nanocomposites with ZrO_2 or MgO, the current decreased rapidly to zero, meaning that the electronic conductivity is negligible. However, the sample containing TiO_2 showed a steady-state electronic conductivity of 4.6×10^{-6} S/cm, which explains the low activation energy detected for the overall conductivity. This shows how important it is, in reporting ionic conductivities, to verify whether all conductivity measured by electrochemical impedance spectroscopy is due to ionic conductivity and to exclude the possibility of significant electronic conductivity.

For mixtures with silica, the optimum composition was previously observed to be close to 100% pore filling. Since the pore volume (V_p) of other oxides (see Table 1) is much smaller than that of SiO_2, for all samples, the fraction of pore filling is much higher than 100%. Therefore, it is likely that even much higher conductivities can be obtained in these $LiBH_4$–oxide systems when using an optimum ratio between $LiBH_4$ and oxide.

For practical applications, the electrochemical stability window is very important. For pure $LiBH_4$, it is reported to be around 2 V vs. Li^+/Li.[9,10] All-solid-state Li-ion batteries have been prepared using a $LiBH_4$–nanoporous SiO_2 nanocomposite as a solid-state electrolyte, showing the potential of this type of electrolyte for application in full-cell batteries.[23,48,50]

CONCLUSIONS

We explored the effect of adding various nanosized oxides by ball-milling on the solid-state ion conductivity of $LiBH_4$. First, the effect of heat cycling up to 130 °C was investigated. While for the pure ball-milled $LiBH_4$ the conductivity gradually decreased upon temperature cycling, for the oxide-containing nanocomposites, the conductivity actually increased upon the first temperature cycle and remained remarkably stable upon further cycling. The presence of oxide nanoparticles in the nanocomposite for all oxides investigated greatly enhanced the ionic conductivity, typically with about 3 orders of magnitude at 40 °C. $LiBH_4$–SiO_2 nanocomposites have been reported before, but we investigated in detail the effect of structural properties and composition on the conductivity. This led to a few guidelines to reach the maximum conductivity in these nanocomposites

(1) The volume of $LiBH_4$ in the nanocomposite should correspond roughly to the pore volume of the oxide powder before ball-milling.

(2) A heat cycle to 130 °C (slightly above the solid–solid phase transition temperature) is effective for reaching maximum conductivity, which is stable upon repeated temperature cycling.

(3) Although the highest conductivity is found within 2 nm of the $LiBH_4$/oxide interface, nanocomposites with an average $LiBH_4$ thickness of 5–8 nm on the oxide (as calculated using the oxide BET surface area) give the highest conductivities, which are not limited by low-conductivity macrocrystalline $LiBH_4$ regions. If possible, the porosity of the oxide should be adjusted to optimize this factor.

(4) The nature of the oxide is important. Nanocomposites with SiO_2 and Al_2O_3 had been reported before, but the highest conductivities (0.26 and 0.18 mS/cm at 40 °C) were observed for nanocomposites with ZrO_2 and MgO,

https://dx.doi.org/10.1021/acsaem.9b02268
ACS Appl. Energy Mater. 2020, 3, 4941–4948

respectively, while these conductivities can be further increased by optimizing the composition and morphology. Care has to be taken with reducible oxides like TiO_2, as high conductivities can be partially ascribed to electronic conductitvity, due to partial reduction of the oxide by $LiBH_4$.

These general insights into optimal structural parameters are probably relevant for any $LiBH_4$–oxide system, although of course it remains important to also practically test the different compositions in full solid-state Li-ion batteries. We feel that these insights and guidelines may be useful in developing solid-state ion conductors, for instance, for next-generation all-solid-state Li-ion batteries.

■ ASSOCIATED CONTENT

Supporting Information

The Supporting Information is available free of charge at https://pubs.acs.org/doi/10.1021/acsaem.9b02268.

XRD and HP-DSC measurements for pure and ball-milled $LiBH_4$ as well as for the $LiBH_4$/oxide nanocomposites. Additional overall and electronic conductivity data are presented, including Nyquist plots and the equivalent circuits used to fit the obtained data. (PDF)

■ AUTHOR INFORMATION

Corresponding Authors

Marcello Baricco − *Department of Chemistry and Interdepartmental Center Nanostructured Interfaces and Surfaces (NIS), University of Turin, 10125 Torino, Italy;* orcid.org/0000-0002-2856-9894; Email: marcello.baricco@unito.it

Petra E. de Jongh − *Inorganic Chemistry and Catalysis, Debye Institute for Nanomaterials Science, Utrecht University, 3584 CG Utrecht, The Netherlands;* orcid.org/0000-0002-2216-2620; Email: P.E.deJongh@uu.nl

Authors

Valerio Gulino − *Department of Chemistry and Interdepartmental Center Nanostructured Interfaces and Surfaces (NIS), University of Turin, 10125 Torino, Italy*

Laura Barberis − *Department of Chemistry and Interdepartmental Center Nanostructured Interfaces and Surfaces (NIS), University of Turin, 10125 Torino, Italy; Inorganic Chemistry and Catalysis, Debye Institute for Nanomaterials Science, Utrecht University, 3584 CG Utrecht, The Netherlands*

Peter Ngene − *Inorganic Chemistry and Catalysis, Debye Institute for Nanomaterials Science, Utrecht University, 3584 CG Utrecht, The Netherlands;* orcid.org/0000-0003-3691-0623

Complete contact information is available at: https://pubs.acs.org/10.1021/acsaem.9b02268

Author Contributions

#V.G. and L.B. are cofirst authors.

Notes

The authors declare no competing financial interest.

■ ACKNOWLEDGMENTS

Financial support from The Netherlands Organisation for Scientific Research (NWO-ECHO) is gratefully acknowledged. V.G. and L.B. thank the Erasmus Traineeship Programme for the financial support in the exchange mobility period between the University of Utrecht and the University of Turin. The authors kindly acknowledge Sander Lambregts, Laura de Kort, and Jan Willem de Rijk for technical support in the laboratory.

■ REFERENCES

(1) Xu, K. Nonaqueous Liquid Electrolytes for Lithium-Based Rechargeable Batteries. *Chem. Rev.* **2004**, *104* (10), 4303–4417.

(2) Bachman, J. C.; Muy, S.; Grimaud, A.; Chang, H.-H.; Pour, N.; Lux, S. F.; Paschos, O.; Maglia, F.; Lupart, S.; Lamp, P.; Giordano, L.; Shao-Horn, Y. Inorganic Solid-State Electrolytes for Lithium Batteries: Mechanisms and Properties Governing Ion Conduction. *Chem. Rev.* **2016**, *116* (1), 140–162.

(3) Manthiram, A.; Yu, X.; Wang, S. Lithium Battery Chemistries Enabled by Solid-State Electrolytes. *Nat. Rev. Mater.* **2017**, *2* (4), 16103.

(4) Tarascon, J.-M.; Armand, M. Issues and Challenges Facing Rechargeable Lithium Batteries. *Nature* **2001**, *414* (6861), 359–367.

(5) Matsuo, M.; Orimo, S. Lithium Fast-Ionic Conduction in Complex Hydrides: Review and Prospects. *Adv. Energy Mater.* **2011**, *1* (2), 161–172.

(6) Duchêne, L.; Kühnel, R.-S.; Stilp, E.; Cuervo Reyes, E.; Remhof, A.; Hagemann, H.; Battaglia, C. A Stable 3 V All-Solid-State Sodium–Ion Battery Based on a Closo -Borate Electrolyte. *Energy Environ. Sci.* **2017**, *10* (12), 2609–2615.

(7) Unemoto, A.; Yoshida, K.; Ikeshoji, T.; Orimo, S. Bulk-Type All-Solid-State Lithium Batteries Using Complex Hydrides Containing Cluster-Anions. *Mater. Trans.* **2016**, *57* (9), 1639–1644.

(8) Tang, W. S.; Unemoto, A.; Zhou, W.; Stavila, V.; Matsuo, M.; Wu, H.; Orimo, S. I.; Udovic, T. J. Unparalleled Lithium and Sodium Superionic Conduction in Solid Electrolytes with Large Monovalent Cage-like Anions. *Energy Environ. Sci.* **2015**, *8* (12), 3637–3645.

(9) Asakura, R.; Duchêne, L.; Kühnel, R.-S.; Remhof, A.; Hagemann, H.; Battaglia, C. Electrochemical Oxidative Stability of Hydroborate-Based Solid-State Electrolytes. *ACS Appl. Energy Mater.* **2019**, *2* (9), 6924–6930.

(10) Gulino, V.; Brighi, M.; Dematteis, E. M.; Murgia, F.; Nervi, C.; Černý, R.; Baricco, M. Phase Stability and Fast Ion Conductivity in the Hexagonal $LiBH_4$–LiBr–LiCl Solid Solution. *Chem. Mater.* **2019**, *31* (14), 5133–5144.

(11) Matsuo, M.; Nakamori, Y.; Orimo, S.; Maekawa, H.; Takamura, H. Lithium Superionic Conduction in Lithium Borohydride Accompanied by Structural Transition. *Appl. Phys. Lett.* **2007**, *91* (22), 224103.

(12) Soulie, J.; Renaudin, G.; Černý, R.; Yvon, K. Lithium Boro-Hydride $LiBH_4$ I. Crystal Structure. *J. Alloys Compd.* **2002**, *346*, 200–205.

(13) Rude, L. H.; Groppo, E.; Arnbjerg, L. M.; Ravnsbæk, D. B.; Malmkjær, R. A.; Filinchuk, Y.; Baricco, M.; Besenbacher, F.; Jensen, T. R. Iodide Substitution in Lithium Borohydride, $LiBH_4$–LiI. *J. Alloys Compd.* **2011**, *509* (33), 8299–8305.

(14) Rude, L. H.; Zavorotynska, O.; Arnbjerg, L. M.; Ravnsbæk, D. B.; Malmkjær, R. A.; Grove, H.; Hauback, B. C.; Baricco, M.; Filinchuk, Y.; Besenbacher, F.; Jensen, T. R. Bromide Substitution in Lithium Borohydride, $LiBH_4$–LiBr. *Int. J. Hydrogen Energy* **2011**, *36* (24), 15664–15672.

(15) Cascallana-Matias, I.; Keen, D. A.; Cussen, E. J.; Gregory, D. H. Phase Behavior in the $LiBH_4$–LiBr System and Structure of the Anion-Stabilized Fast Ionic, High Temperature Phase. *Chem. Mater.* **2015**, *27* (22), 7780–7787.

(16) Maekawa, H.; Matsuo, M.; Takamura, H.; Ando, M.; Noda, Y.; Karahashi, T.; Orimo, S. Halide-Stabilized $LiBH_4$, a Room-Temperature Lithium Fast-Ion Conductor. *J. Am. Chem. Soc.* **2009**, *131* (3), 894–895.

(17) Sveinbjörnsson, D.; Myrdal, J. S. G.; Blanchard, D.; Bentzen, J. J.; Hirata, T.; Mogensen, M. B.; Norby, P.; Orimo, S.; Vegge, T. Effect of Heat Treatment on the Lithium Ion Conduction of the $LiBH_4$–LiI Solid Solution. *J. Phys. Chem. C* **2013**, *117* (7), 3249–3257.

(18) Wolczyk, A.; Pinatel, E. R.; Chierotti, M. R.; Nervi, C.; Gobetto, R.; Baricco, M. Solid-State NMR and Thermodynamic

Investigations on $LiBH_4LiNH_2$ System. *Int. J. Hydrogen Energy* **2016**, *41* (32), 14475−14483.
(19) Matsuo, M.; Remhof, A.; Martelli, P.; Caputo, R.; Ernst, M.; Miura, Y.; Sato, T.; Oguchi, H.; Maekawa, H.; Takamura, H.; Borgschulte, A.; Züttel, A.; Orimo, S. Complex Hydrides with $(BH_4)^-$ and $(NH_2)^-$ Anions as New Lithium Fast-Ion Conductors. *J. Am. Chem. Soc.* **2009**, *131* (45), 16389−16391.
(20) Wolczyk, A.; Paik, B.; Sato, T.; Nervi, C.; Brighi, M.; GharibDoust, S. P.; Chierotti, M.; Matsuo, M.; Li, G.; Gobetto, R.; Jensen, T. R.; Černý, R.; Orimo, S.; Baricco, M. $Li_5(BH_4)_3NH$: Lithium-Rich Mixed Anion Complex Hydride. *J. Phys. Chem. C* **2017**, *121* (21), 11069−11075.
(21) Fichtner, M. Nanoconfinement Effects in Energy Storage Materials. *Phys. Chem. Chem. Phys.* **2011**, *13* (48), 21186.
(22) Choi, Y. S.; Lee, Y.-S.; Oh, K. H.; Cho, Y. W. Interface-Enhanced Li Ion Conduction in a $LiBH_4−SiO_2$ Solid Electrolyte. *Phys. Chem. Chem. Phys.* **2016**, *18* (32), 22540−22547.
(23) Verkuijlen, M. H. W.; Ngene, P.; de Kort, D. W.; Barré, C.; Nale, A.; van Eck, E. R. H.; van Bentum, P. J. M.; de Jongh, P. E.; Kentgens, A. P. M. Nanoconfined $LiBH_4$ and Enhanced Mobility of Li^+ and BH_4^- Studied by Solid-State NMR. *J. Phys. Chem. C* **2012**, *116* (42), 22169−22178.
(24) Suwarno; Ngene, P.; Nale, A.; Eggenhuisen, T. M.; Oschatz, M.; Embs, J. P.; Remhof, A.; De Jongh, P. E. Confinement Effects for Lithium Borohydride: Comparing Silica and Carbon Scaffolds. *J. Phys. Chem. C* **2017**, *121* (8), 4197−4205.
(25) Choi, Y. S.; Lee, Y.-S.; Choi, D.-J.; Chae, K. H.; Oh, K. H.; Cho, Y. W. Enhanced Li Ion Conductivity in $LiBH_4−Al_2O_3$ Mixture via Interface Engineering. *J. Phys. Chem. C* **2017**, *121* (47), 26209−26215.
(26) Lefevr, J.; Cervini, L.; Griffin, J. M.; Blanchard, D. Lithium Conductivity and Ions Dynamics in $LiBH_4/SiO_2$ Solid Electrolytes Studied by Solid-State NMR and Quasi-Elastic Neutron Scattering and Applied in Lithium−Sulfur Batteries. *J. Phys. Chem. C* **2018**, *122* (27), 15264−15275.
(27) Blanchard, D.; Nale, A.; Sveinbjörnsson, D.; Eggenhuisen, T. M.; Verkuijlen, M. H. W.; Suwarno; Vegge, T.; Kentgens, A. P. M.; de Jongh, P. E. Nanoconfined $LiBH_4$ as a Fast Lithium Ion Conductor. *Adv. Funct. Mater.* **2015**, *25* (2), 184−192.
(28) Verdal, N.; Udovic, T. J.; Rush, J. J.; Liu, X.; Majzoub, E. H.; Vajo, J. J.; Gross, A. F. Dynamical Perturbations of Tetrahydroborate Anions in $LiBH_4$ Due to Nanoconfinement in Controlled-Pore Carbon Scaffolds. *J. Phys. Chem. C* **2013**, *117* (35), 17983−17995.
(29) Ngene, P.; Adelhelm, P.; Beale, A. M.; de Jong, K. P.; de Jongh, P. E. $LiBH_4$/SBA-15 Nanocomposites Prepared by Melt Infiltration under Hydrogen Pressure: Synthesis and Hydrogen Sorption Properties. *J. Phys. Chem. C* **2010**, *114*, 6163−6168.
(30) Indris, S.; Heitjans, P. Heterogeneous ^7Li NMR Relaxation in Nanocrystalline $Li_2O:B_2O_3$ Composites. *J. Non-Cryst. Solids* **2002**, *307*−*310* (3), 555−564.
(31) Wilkening, M.; Indris, S.; Heitjans, P. Heterogeneous Lithium Diffusion in Nanocrystalline $Li_2O:Al_2O_3$ Composites. *Phys. Chem. Chem. Phys.* **2003**, *5* (11), 2225−2231.
(32) Indris, S.; Heitjans, P.; Roman, H. E.; Bunde, A. Nanocrystalline versus Microcrystalline Composites: Anomalous Ionic Conductivities and Percolation Theory. *Phys. Rev. Lett.* **2000**, *84* (13), 2889−2892.
(33) Breuer, S.; Pregartner, V.; Lunghammer, S.; Wilkening, H. M. R. Dispersed Solid Conductors: Fast Interfacial Li-Ion Dynamics in Nanostructured LiF and LiF:γ-Al_2O_3 Composites. *J. Phys. Chem. C* **2019**, *123* (9), 5222−5230.
(34) Epp, V.; Wilkening, M. Motion of Li^+ in Nanoengineered $LiBH_4$ and $LiBH_4:Al_2O_3$ Comparison with the Microcrystalline Form. *ChemPhysChem* **2013**, *14* (16), 3706−3713.
(35) Maier, J. Ionic Conduction in Space Charge Regions. *Prog. Solid State Chem.* **1995**, *23* (3), 171−263.
(36) Liu, X.; Majzoub, E. H.; Stavila, V.; Bhakta, R. K.; Allendorf, M. D.; Shane, D. T.; Conradi, M. S.; Verdal, N.; Udovic, T. J.; Hwang, S.-J. Probing the Unusual Anion Mobility of $LiBH_4$ Confined in Highly Ordered Nanoporous Carbon Frameworks via Solid State NMR and Quasielastic Neutron Scattering. *J. Mater. Chem. A* **2013**, *1* (34), 9935.
(37) Dimitrov, V.; Sakka, S. Electronic Oxide Polarizability and Optical Basicity of Simple Oxides. I. *J. Appl. Phys.* **1996**, *79* (3), 1736−1740.
(38) Brunauer, S.; Emmett, P. H.; Teller, E. Adsorption of Gases in Multimolecular Layers. *J. Am. Chem. Soc.* **1938**, *60* (2), 309−319.
(39) Boukamp, B. A. Electrochemical Impedance Spectroscopy in Solid State Ionics: Recent Advances. *Solid State Ionics* **2004**, *169* (1−4), 65−73.
(40) Boukamp, B. A. A Package for Impedance/Admittance Data Analysis. *Solid State Ionics* **1986**, *19*, 136−140.
(41) Matsuo, M.; Takamura, H.; Maekawa, H.; Li, H.-W.; Orimo, S. Stabilization of Lithium Superionic Conduction Phase and Enhancement of Conductivity of $LiBH_4$ by LiCl Addition. *Appl. Phys. Lett.* **2009**, *94* (8), 084103.
(42) Sveinbjörnsson, D.; Blanchard, D.; Myrdal, J. S. G.; Younesi, R.; Viskinde, R.; Riktor, M. D.; Norby, P.; Vegge, T. Ionic Conductivity and the Formation of Cubic CaH_2 in the $LiBH_4−Ca(BH_4)_2$ Composite. *J. Solid State Chem.* **2014**, *211*, 81−89.
(43) Breuer, S.; Uitz, M.; Wilkening, H. M. R. Rapid Li Ion Dynamics in the Interfacial Regions of Nanocrystalline Solids. *J. Phys. Chem. Lett.* **2018**, *9* (8), 2093−2097.
(44) Breuer, S.; Uitz, M.; Wilkening, H. M. R. Rapid Li Ion Dynamics in the Interfacial Regions of Nanocrystalline Solids. *J. Phys. Chem. Lett.* **2018**, *9* (8), 2093−2097.
(45) Ngene, P.; Lambregts, S. F. H.; Blanchard, D.; Vegge, T.; Sharma, M.; Hagemann, H.; de Jongh, P. E. The Influence of Silica Surface Groups on the Li-Ion Conductivity of $LiBH_4/SiO_2$ Nanocomposites. *Phys. Chem. Chem. Phys.* **2019**, *21* (40), 22456−22466.
(46) Barzan, C.; Groppo, E.; Bordiga, S.; Zecchina, A. Defect Sites in H_2-Reduced TiO_2 Convert Ethylene to High Density Polyethylene without Activator. *ACS Catal.* **2014**, *4* (3), 986−989.
(47) Kim, K. H.; Oh, E. J.; Choi, J. S. Electrical Conductivity of "Hydrogen-Reduced" Titanium Dioxide (Rutile). *J. Phys. Chem. Solids* **1984**, *45* (11−12), 1265−1269.
(48) Das, S.; Ngene, P.; Norby, P.; Vegge, T.; de Jongh, P. E.; Blanchard, D. All-Solid-State Lithium-Sulfur Battery Based on a Nanoconfined $LiBH_4$ Electrolyte. *J. Electrochem. Soc.* **2016**, *163* (9), A2029−A2034.
(49) Agrawal, R. C. Dc Polarisation: An Experimental Tool in the Study of Ionic Conductors. *Indian J. Pure Appl. Phys.* **1999**, *37* (4), 294−301.
(50) Latroche, M.; Blanchard, D.; Cuevas, F.; El Kharbachi, A.; Hauback, B. C.; Jensen, T. R.; de Jongh, P. E.; Kim, S.; Nazer, N. S.; Ngene, P.; Orimo, S.; Ravnsbæk, D. B.; Yartys, V. A.; et al. Full-Cell Hydride-Based Solid-State Li Batteries for Energy Storage. *Int. J. Hydrogen Energy* **2019**, *44* (15), 7875−7887.

https://dx.doi.org/10.1021/acsaem.9b02268
ACS Appl. Energy Mater. 2020, 3, 4941−4948